

Use of the iNo score to discriminate normal from altered nucleolar morphology, with applications in basic cell biology and potential in human disease diagnostics

Vassiliki Stamatopoulou¹, Pascaline Parisot², Christophe De Vleeschouwer² and Denis L. J. Lafontaine^{3*}

Ribosome biogenesis is initiated in the nucleolus, a cell condensate essential to gene expression, whose morphology informs cancer pathologists on the health status of a cell. Here, we describe a protocol for assessing, both qualitatively and quantitatively, the involvement of *trans*-acting factors in the nucleolar structure. The protocol involves use of siRNAs to deplete cells of factors of interest, fluorescence imaging of nucleoli in an automated high-throughput platform, and use of dedicated software to determine an index of nucleolar disruption, the iNo score. This scoring system is unique in that it integrates the five most discriminant shape and textural features of the nucleolus into a parametric equation. Determining the iNo score enables both qualitative and quantitative factor classification with prediction of function (functional clustering), which to our knowledge is not achieved by competing approaches, as well as stratification of their effect (severity of defects) on nucleolar structure. The iNo score has the potential to be useful in basic cell biology (nucleolar structure–function relationships, mitosis, and senescence), developmental and/or organismal biology (aging), and clinical practice (cancer, viral infection, and reproduction). The entire protocol can be completed within 1 week.

Introduction

The nucleolus is a highly dynamic nuclear subcompartment whose morphology varies greatly in response to stress, disease, and aging. This morphological sensitivity to environmental inputs makes the nucleolus a potent biomarker^{1,2}. Recently, we developed a novel technique for characterizing nucleolar morphological features in both quantitative and qualitative terms³. Our approach is innovative in that it proposes, for the first time, a statistically validated numerical index describing nucleolar morphology. We have called our numerical index the ‘iNo score’ for index of nucleolar disruption. An advantage over previously introduced semiquantitative methods of nucleolar structure characterization is that the iNo score integrates the five most discriminant shape and textural features of the nucleolus. In fact, previous methods took into consideration only the area or pixel intensity of the nucleoli or the number of nucleoli per cell, which does not enable qualitative discrimination of nucleolar disruption to be performed.

As a proof of concept, we systematically examined the involvement of the 80 human ribosomal proteins (r-proteins) in maintaining nucleolar structure, ranking them according to how strongly their depletion affects this structure³. Incidentally, we found that the r-proteins that influence nucleolar structure the most all assemble onto the maturing large ribosomal subunit at a late stage of ribosome biogenesis. Remarkably, this observation establishes a clear correlation between individual steps of ribosome biogenesis (late assembly of the large ribosomal subunit) and the formation of microscopically detectable subcellular structures (a well-organized nucleolus).

We believe that our technique has great potential in medical and clinical research because nucleolar biology reflects the health of a cell. The shape and size of the nucleolus, and the number of nucleoli per cell vary greatly in response to diseases such as cancer⁴, upon viral infection⁵, and in the course of life (aging)⁶. Additional applications are anticipated in clinical practice. In human

¹Department of Biochemistry, School of Medicine, University of Patras, Patras, Greece. ²ICTEAM-ELEN, Université Catholique de Louvain, Louvain-la-Neuve, Belgium. ³RNA Molecular Biology, F.R.S./FNRS, Université Libre de Bruxelles, Charleroi-Gosselies, Belgium. *e-mail: denis.lafontaine@ulb.ac.be

reproduction, for example, the observation of nucleolar characteristics of embryos is used to evaluate the developmental potential of human zygotes⁷. We believe that the iNo score has wide-ranging applicability. Using the protocol described here, it should be possible to implement our fully standardized and calibrated procedure in both academic research laboratories and clinical biology settings.

Here, we present a fully detailed, user-friendly, hands-on version of our approach, including a training dataset, examples of applications, and a comparison with preexisting, mostly nonquantitative methods.

Development and overview of the protocol

Considerations related to both clinical and basic cell biology prompted us to design a method for precisely stratifying nucleolar disruption. Notably, the size, shape, and number of nucleoli per cell vary greatly between healthy and pathological states. Yet pathologists do not widely exploit nucleolar structure because of the lack of reliable assays that can be routinely implemented in a clinical setting. On the other hand, the principles governing nucleolar integrity during the interphase and nucleolar disassembly–reassembly during mitosis have remained largely unknown⁸. The aim of our technique was thus to identify cell components that are important in nucleolar structure maintenance during the interphase and in nucleolar disassembly–reassembly at the beginning and at the end of mitosis, respectively. We also aimed to characterize nucleolar disruption both qualitatively and quantitatively to provide support to both academic research and clinical diagnosis.

To distinguish the nucleoli of a population of cells depleted of a cellular component from those of a population of control cells, the present approach introduces the iNo score as the L1-norm of a discrepancy vector whose components reflect the distances between the distributions of discriminant morphometric features in the two cell populations. Mathematically, the L1-norm of a vector denotes the sum of the absolute values of its components, and the distance between the two distributions is measured by their mean difference normalized by their quadratic mean. The iNo score ranges from 0.00 (no defect in the nucleolar structure) to 0.25 (severely damaged nucleolus). To group together the cellular components whose depletion leads to similar nucleolar disruption ('functional clustering', i.e., the qualitative aspect of our protocol), principal component analysis (PCA) of the discrepancy vector is performed.

As proof-of-concept, we tested the influence of the 80 human r-proteins on nucleolar structure maintenance, depleting cells of each one individually (<http://www.ribosomalproteins.com>). The rationale for this approach was: (i) r-proteins are highly abundant; (ii) most r-proteins assemble onto maturing ribosomal subunits in the nucleolus; (iii) r-proteins are frequently mutated in ribosomopathies (syndromes caused by ribosome biogenesis dysfunction often associated with cancer predisposition); and (iv) several r-proteins play a direct role in the homeostasis of cancer-related proteins, such as p53 and the retinoblastoma protein (pRB). These facts led us to rank the r-proteins with respect to their importance in nucleolar structure maintenance. Surprisingly, it appeared that, although most r-proteins assemble onto nascent precursor ribosomes in the nucleolus, very few are required for maintaining its internal architecture³. Specifically, we found only late-assembling r-proteins of the large subunit to be important in nucleolar structure maintenance. To further illustrate our protocol, we have now tested 668 additional abundant nucleolar proteins, revealing that ~40% of them influence nucleolar architecture (V.S., P.P., C.D.V., and D.L.J.L., data not shown; see also Anticipated results).

Our method consists of five main stages (Fig. 1), which will be discussed further in the following paragraphs: (i) gene expression perturbation and preparation of the screening plates (Steps 1–17, optional Box 1); (ii) high-throughput image acquisition (Steps 18–26); (iii) image processing, segmentation, and feature extraction (Steps 27–30 and steps 1 and 2 of Box 2); (iv) statistical analysis (PCA) and prediction of factor function (Box 2, step 3); and (v) iNo score computation and factor ranking (Box 2, step 4).

Stage 1

Stage 1 includes gene expression perturbation and preparation of the screening plates (Steps 1–17 and optional Box 1). To induce nucleolar disruption experimentally, we use siRNA-mediated depletion of the expression of target genes (note that siRNAs target mRNAs, triggering their degradation). Our nucleolar screens are performed on 96-well plates that have a glass bottom that facilitates microscopy-based observation (Reagents). A reporter cell line producing the nucleolar protein fibrillarin (FBL)

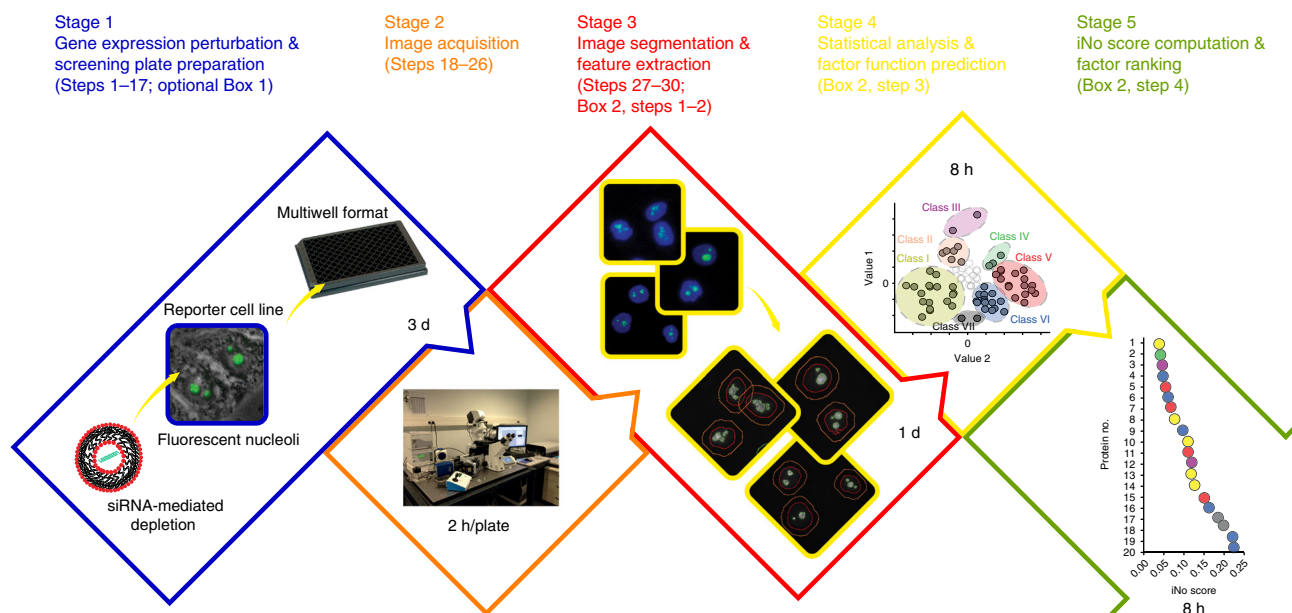


Fig. 1 | High-throughput screening pipeline for identifying factors involved in nucleolar structure maintenance. The Procedure includes five main stages: stage 1, adaptable to a high-throughput format, involves perturbation of the expression of a chosen gene (by, e.g., RNAi-mediated depletion or CRISPR–Cas9 genome editing) in a reporter cell line expressing a suitable fluorescently tagged nucleolar protein (e.g., fibrillarin (FBL); alternatively, an endogenously expressed nucleolar protein can be detected by immunofluorescence); in stage 2, once fixed, the samples are processed for imaging on a high-throughput microscopy platform (typically at 20 \times , with 16 captures per well of a 96-well plate); in stage 3, the captured images are processed and segmented to highlight individual nuclei and nucleoli, and features are extracted; in stage 4, statistical analysis and functional clustering are performed with dedicated software, and the function of factors can be predicted; in stage 5, an iNo score or index of nucleolar disruption is computed, and factors are ranked according to their importance in nucleolar structure maintenance. The step numbers and approximate duration of each stage are indicated as a reference.

Box 1 | Immunofluorescence staining of a human cell line for the detection of one (e.g., PES1) or several nucleolar proteins ● **Timing** 5 h 30 min for a 96-well plate

- 1 Permeabilize the membranes of the fixed cells from Step 11 of the Procedure by adding 100 μ l of 0.2% (vol/vol) Triton X-100 and 2% (wt/vol) BSA solution to each well and incubate the plate for 10 min on ice. Remove and discard the solution from the wells.
- 2 To wash the plate, add 1 \times PBS/2% (wt/vol) BSA to each well and then incubate the plate for 10 min on ice. Repeat for a total of three washes. Remove and discard the solution from the wells.
▲ **CRITICAL STEP** Remove the wash solution with a pipette and do not aspirate. Aspiration will cause loss of cells.
- 3 Add to each well 100 μ l of 1 \times PBS/2% (wt/vol) BSA and incubate the plate at room temperature (23 $^{\circ}$ C) for 30 min to prevent any nonspecific binding of the antibodies. Remove and discard the solution from the wells.
- 4 Add to each well 100 μ l of a freshly made 1:1,000 dilution of your primary antibody (in our case, anti-PES1 raised in rat) in 1 \times PBS/2% (wt/vol) BSA and incubate the plate for 1 h at room temperature in a humidified chamber. Remove and discard the solution from the wells.
- 5 To wash the plate, add 1 \times PBS/2% (wt/vol) BSA to each well and then incubate the plate for 10 min on ice. Repeat for a total of three washes. Remove and discard the solution from the wells.
- 6 Add to each well 100 μ l of a freshly made 1:1,000 dilution of fluorescently labeled secondary antibody (in our case, anti-rat Alexa Fluor 568 raised in goat) in 1 \times PBS/2% (wt/vol) BSA. Incubate the plate for 1 h at room temperature in a humidified chamber. Remove and discard the solution from the wells.
▲ **CRITICAL STEP** Protect the plate from light to avoid photobleaching the fluorochrome of the secondary antibody.
- 7 To wash the plate, add 1 \times PBS to each well and then incubate the plate at room temperature for 10 min. Repeat for a total of four washes, remove and discard the solution from the wells, and then proceed to Step 12 of the main Procedure.

bearing a green fluorescent tag is used. FBL is a methyltransferase associated with box C/D small nucleolar RNA (snRNA), which is involved in the early steps of ribosome maturation (early pre-ribosomal RNA processing and 2'-O-methylation of rRNAs), and it localizes mainly in the dense fibrillar component (DFC) of the nucleolus (the middle of the three layers of the nucleolus)⁸.

Box 2 | Four subscripts of the script 's_main.m' in MATLAB

1 The script 's_compute_segmentation.m' segments the nuclei in all the images of the database. The segmentation masks are saved in the directory 'results/bw/', according to the same hierarchy as used in the initial database: one subdirectory per plate. The name of each segmented image is as follows: 'X_Y_sZ_bw.png', in which X, Y, and Z are the same parameters defined in Step 28.

▲ CRITICAL STEP Optionally, when the procedure followed to generate the library of images (Steps 1–26) differs substantially from that described above and results in nucleolar images characterized by substantially weaker or stronger fluorescence intensity than the images expected from this protocol (for comparable cell components), we recommend adapting the morphometric feature parameters to the data at hand. To achieve this goal, perform step 1 of Box 2 ('s_compute_segmentation.m') and then run the script 's_optimize_parameters.m'. This script takes as inputs a list of well's indices, as defined by the variable 'index_wells_for_opti' in 's_optimize_parameters.m'. These indices identify the wells whose cells will be compared with the control cells during optimization. We recommend selecting a set of wells that is representative of the visual disruption observed in the image samples (such as the calibration set). The script assumes that those wells have already been segmented (by means of 's_compute_segmentation.m', step 1 of Box 2). It generates a number of plots depicting the discriminative power of a feature of interest as a function of one or two parameters. The discriminative power is measured as Fisher's scoring between the distributions of features observed in populations of depleted and control cells (discussed in Nicolas et al.³). The plots are saved in the 'figures_parameters_optimization' directory. The optimal parameters for the dataset at hand are those corresponding to the highest (maximal) discriminative power values in each plot. They can easily be selected manually from the two-dimensional or three-dimensional plots and should be encoded in the header of 's_compute_all_features.m' (used in step 2 of Box 2), instead of the default values.

? TROUBLESHOOTING

2 The script 's_compute_all_features.m' computes, for each of the segmented nuclei, the five nucleolar morphometric features that have been selected in Nicolas et al.³. The features are computed from the GFP images. For each well, the features associated with each individual nucleus are saved in the directory 'results/features' under the filename 'res_XYZ_features.mat', in which X, Y, and Z are the parameters defined above. The numbers of nuclei per well are saved in the 'results' directory in the file 'nb_nuclei_by_well.mat'.

▲ CRITICAL STEP Alternatively, the entire set of 13 features discussed in Nicolas et al.³ may be computed by setting the 'compute_all_features' flag to 1 in the 'dataconfig.m' file. We have observed, however, that these features are redundant, in the sense that they are correlated with the five recommended features, making their computation unnecessary.

▲ CRITICAL STEP Additional parameterized features could be added to the set of 13 morphometric features considered in Nicolas et al.³ so as to reflect the visual differences observed between the populations of nucleoli from the control and protein-depleted cells. This approach would of course require the design and implementation of additional scripts.

▲ CRITICAL STEP As discussed in Nicolas et al.³, the parameters associated with a given feature are defined so as to maximize the distance between the distributions of the features in protein-depleted cells and SCR-treated control cells. Their default values, encoded in the header of the 's_compute_all_features.m' file, have been computed from the dataset investigated in Nicolas et al.³, generated using this protocol. We found these default parameters to be robust, as they appeared correct for two completely independent datasets (Nicolas et al.³ and Fig. 2) collected with the same microscope and acquisition software, but using different cells manipulated by another biologist after an interval of several months. The first dataset aimed at testing the involvement of the 80 human r-proteins in nucleolar structure (Nicolas et al.³), whereas the second dataset aimed at testing the involvement of 668 abundant human nucleolar proteins in the morphology of the organelle (Fig. 2). Despite the robustness of our default parameters, it might be necessary to optimize them to the imaging setup (camera), which converts the nucleolar components into pixel intensities. The parameters correspond to a set of thresholds defining how to segment the GFP signal into the individual nucleolar components from which nonparametric features are computed. To adapt the values of these parameters to the experimental data at hand, therefore, the script 's_optimize_parameters.m' may be run before this step if necessary, as detailed above.

3 The script 's_compute_all_distances.m' computes the discrepancy vector for each population of cells depleted of a given protein of interest. As discussed in Nicolas et al.³, each component of the discrepancy vector is associated with a specific nucleolar morphometric feature and a Fisher's score computed between the distributions of this feature for a protein-depleted population and for a nondepleted control population. A population is defined on a 'per well' basis, which means that the nucleoli observed at all sites in a given well are pooled to define a population distribution. The components of the discrepancy vector computed for each well are saved in the file 'all_the_distances.mat' in the 'results' directory.

4 The script 's_analyze_features_vectors.m' computes the iNo score associated with each protein of interest and sorts the proteins by the severity of their effect on the nucleoli. It also performs the PCA of the discrepancy vectors, each vector being derived for a gene of interest on a 'per well' basis. The iNo scores are saved in the 'results/images' directory. The PCA eigenvectors and eigenvalues and the discrepancy vector PCA coefficients are stored in the same directory.

? TROUBLESHOOTING

The reporter cell line is seeded into each well and reverse transfected with an siRNA (Fig. 1). For each target protein, three individual siRNAs are used in three independent experiments. Notably, all screens are performed in triplicate for consistency.

Stage 2

Stage 2 encompasses image acquisition (Steps 18–26). Microscopic images are acquired in wide-field mode on an automated high-throughput screening platform assembled for this specific purpose or a ‘ready-to-use’ commercial equivalent (Equipment; Fig. 1). Sixteen images are acquired for each well of each 96-well screening plate. In our setup, it takes 2 h to image one plate. For consistency, all screens are performed in triplicate. Further details on the hardware used are provided in the ‘Materials’ section.

Stage 3

Stage 3 comprises image processing, segmentation, and feature extraction (Steps 27–30 and Box 2, steps 1–2). To characterize nucleolar morphology defects both qualitatively and quantitatively, we developed a specific image-processing algorithm³ (available for download at <https://github.com/LaFontaineLab/iNo-score>). Briefly, the algorithm initially utilizes shape- and size-consistent adaptive thresholding of a nuclear stain (DAPI) to segment the nuclei being observed (Fig. 1). Then, within each nuclear mass, green fluorescent protein (GFP) signal thresholding and mathematical morphology analysis are applied to segment the nucleoli into connected components. Specifically, a graph is associated with the ‘thresholded’ image by assigning vertices to pixels lying above the threshold and by defining graph edges on the basis of eight-connectivity neighbor relationships between pixels. In this graph, a ‘connected component’ is a subgraph in which each vertex (i.e., each node) is connected to all other vertices in its subgraph but is not connected to any graph vertices lying outside the subgraph. To best discriminate nucleoli in populations of cells depleted of nucleolar proteins from those of control cells (in this case, cells treated with a nontargeting silencer RNA referred to hereafter as scramble or SCR siRNA), a variety of shape and textural parametric features are considered to characterize the largest connected components of each nucleolus. The parameters of each investigated feature are defined to maximize the separation, in terms of Fisher’s criterion, between feature distributions in control cells and those in cells depleted of a candidate protein (step 2 of Box 2). Five features have been selected as the most discriminant ones—in other words, the characteristics that maximize the probabilistic distribution separation—and are used to perform the third stage of the Procedure. These are (i) the area, which denotes the number of pixels, that is the vertices, in the connected component; (ii) the elliptical regularity, defined as the surface ratio between the connected component and the smallest ellipse including the connected component and sharing its principal axes; (iii) the percentage of pixels below an optimized intensity threshold; (iv) the lowest intensity; and (v) the number of local minima, corresponding to the number of pixels lying inside the connected component and whose eight-connectivity neighbors have greater GFP pixel intensity.

Stage 4

Stage 4 constitutes statistical analysis and factor function prediction (Box 2, step 3). For the i th feature and a given population of cells depleted of the k th candidate protein, a statistically significant normalized distance $d_k(i)$ between the protein-depleted and control cell distributions is computed as the ratio of their mean difference to the square root of the sum of their variances. Formally, we have

$$\mathbf{d}_k(i) = \frac{\mu_k(i) - \mu_r(i)}{\sqrt{\sigma_k^2(i) + \sigma_r^2(i)}},$$

where $\mu_r(i)$, $\mu_k(i)$, and $\sigma_r(i)$, $\sigma_k(i)$ denote the mean values and standard deviations of the i th feature distribution derived from two sets of images of nucleoli, one obtained from normal reference cells and one from cells having been depleted of the k th candidate protein.

Each population of candidate-protein-depleted cells is thus characterized by five $\mathbf{d}_k(i)$ values, gathered into a discrepancy vector \mathbf{d}_k . PCA is used to reduce the five dimensions of the discrepancy vector to two, allowing ready visualization of the data in a scatter plot, in which each dot corresponds to a population of cells treated with one siRNA (Figs. 1 and 2a). PCA of the discrepancy vectors is used to extract and visualize the major morphological trends evident in the nucleolus that are associated with depletion of a protein of interest. PCA assumes linear embedding for dimensionality reduction and allows unsupervised clustering of nucleolar disruption phenotypes.

In summary, PCA implementation reveals groups of proteins whose depletion leads to similar nucleolar morphological phenotypes (‘factor clustering’, the qualitative dimension of our analysis), suggesting that they may be involved in the same process and share biological functions.

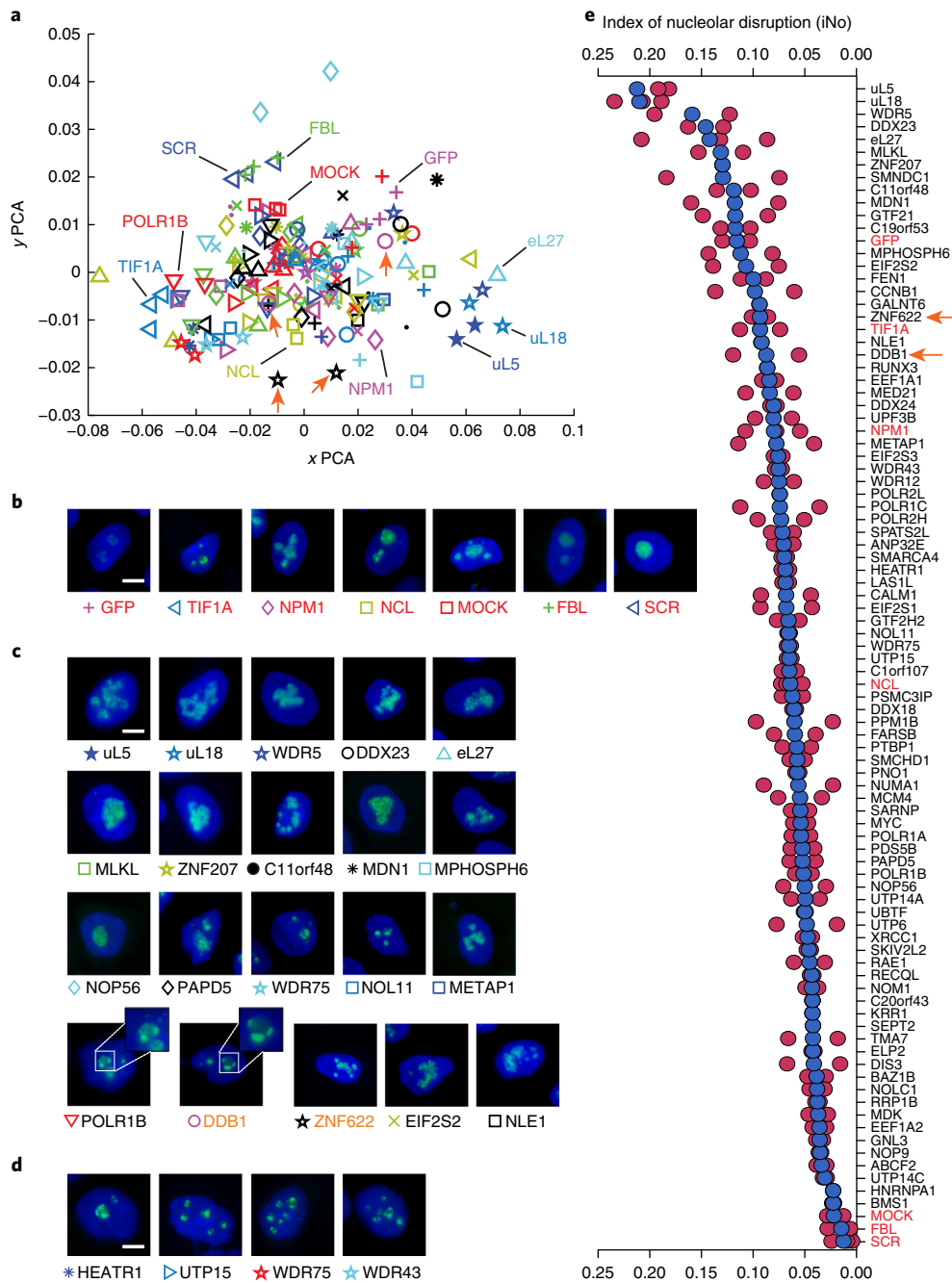


Fig. 2 | Testing the involvement of 86 abundant nucleolar proteins in nucleolar structure maintenance. **a**, Statistical analysis of the results. The graph illustrates a principal component analysis (PCA) in which the five morphological and textural parameters used in our analysis (namely, (i) area, (ii) elliptical regularity, (iii) percentage of pixels below an optimized intensity threshold, (iv) lowest intensity, and (v) number of local minima) have been reduced to two. Each symbol represents a population of (≥ 200) cells depleted of one candidate protein with one siRNA. The large majority of proteins depleted do not strongly impact nucleolar structure, as they appear in the vicinity of the reference controls (SCR, MOCK) in the central area of the graph; however, a few proteins important for nucleolar structure maintenance appear on the periphery of the graph. Identical symbols are often in the immediate vicinity of each other; as identical symbols represent different siRNAs specific to the same target, their proximity on the graph attests to the robustness of the Procedure. Factors used in the calibration set are highlighted on the graph, and orange arrows show two candidates selected for further analysis (DDB1 (pink circles) and ZNF622 (black stars)). Symbols are defined in **b-d**. **b**, Typical images for the calibration set. **c**, To illustrate the diversity of nucleolar phenotypes that one may observe after depletion of specific proteins, representative images are shown. Based on the spectacular disruption of the nucleolus observed after depletion of DDB1 and ZNF622, these proteins were selected for follow-up analysis (Fig. 3 and Supplementary Fig. 1). For POLR1B and DDB1, nucleolar caps are highlighted in 1.7-fold enlargements of the images. **d**, Upon depletion of components of the UTP-A subcomplex of the SSU processome, nucleolar caps are formed in agreement with the role of these proteins in efficient RNA Pol I transcription. **e**, iNo score determination. An iNo score was computed for each candidate protein tested and each siRNA used (red, results for individual siRNAs; blue, mean). The iNo score ranges from 0.00 (no defect in nucleolar structure) to 0.25 (severely damaged nucleolus). Proteins ul5 and ul18 have the highest iNo scores, confirming that they are essential to nucleolar structure maintenance³. The two candidates from **c** selected for follow-up analysis (DDB1 and ZNF622) are highlighted with arrows. The proteins of the calibration set are labeled in red. Scale bars, 5 μ M.

Stage 5

Stage 5 consists of iNo score determination and factor ranking (Box 2, step 4). To stratify the nucleolar proteins according to the severity of the nucleolar disruption caused by their absence (the quantitative aspect of the protocol), we defined an iNo score⁹ as the sum of the absolute values of the five $d_k(i)$ distances, where $0 < i \leq 5$. For each candidate protein, an average iNo score, based on the values obtained with the three different siRNAs used, is calculated and plotted (Figs. 1 and 2e).

In the Procedure, we describe how to implement and use the computer code needed to carry out stages 3–5.

Applications of the protocol

This protocol can be used to investigate essential questions in cell biology, such as those posed in the following paragraphs.

What are the principles governing nucleolar structure maintenance during interphase?

Ribosome biogenesis starts at the core of the organelle, progressing outward. Sequential maturation of the ribosome's subunits leads to the formation of three layers by phase transition^{10,11}. The first layer consists of one or several fibrillar centers (FCs). The second is the DFC surrounding each FC. The third is a single, large granular component (GC), in which the FC/DFC cores are embedded^{8,12}. The exact nature of the reactions occurring in each layer, the RNA and protein compositions of the different layers, and the relationships between them remain largely unclear.

What drives the remarkable nucleolar disassembly–reassembly process occurring during mitosis?

At the onset of mitosis, when RNA polymerase I (RNA Pol I) activity is shut down, the nucleolus disassembles, only to assemble again toward the end of mitosis when transcription resumes. The FC is the first component to dissolve, soon followed by the DFC, and then by the GC⁸. Reassembly of the nucleolus involves the formation of three consecutive intermediary organelles with precursor–product relationships: the peri-chromosomal region (PR), the nucleolus-derived foci, and the prenucleolar bodies. How the formation of these organelles is controlled remains entirely unclear, although Ki-67 has recently been shown to be essential to PR formation¹³.

How generally applicable are novel concepts in cell biology?

With the emergence of novel concepts in cell biology, such as the 'phase transition' model (reviewed in a number of publications^{14–16}), the need for statistically validated methods of image analysis is ever increasing. The phase transition model proposes that dynamic membrane-less organelles such as the nucleolus adopt a liquid–liquid-like behavior involving the de-mixing of the components at the interface between the organelle and its immediate cell environment, such as that which occurs when oil and vinegar are mixed. Such phase transition is influenced by protein and RNA concentrations, electrostatic interactions, temperature, and pH, among other parameters^{10,17}. Experiments aimed at testing the phase transition model induce the formation or the disassembly of natural or synthetic organelles whose level of architecture could typically be characterized with an iNo score.

What is the function of an uncharacterized protein?

Another important benefit of our approach is that it can (to some extent) allow the function of uncharacterized proteins to be predicted on the basis of their functional clustering with factors of known function. In a recent analysis, for example, we found DDB1 to be clustered with RNA Pol I transcription factors (Fig. 2), and we validated the prediction that DDB1 is involved in rRNA synthesis by demonstrating that it interacts with the rDNA locus, where it is required for RNA Pol I function (Anticipated results and Supplementary Fig. 1).

On the basis of the known functions of the nucleolus as a stress sensor whose morphology informs cancer pathologists^{1,4}, our protocol can also be applied to clinical work for diagnostic and prognostic purposes.

Initially, our screens were designed to be conducted with a reporter cell line stably expressing a fluorescently tagged nucleolar marker protein. In clinical practice, naturally, the procedure would have to be adapted to patient cells, which of course do not express such a marker. To date, we have found our screening procedure to be as robust and efficient when used in combination with indirect immunofluorescence detection (with an antibody specific to a nucleolar protein of interest; see Box 1) as when it relies on direct detection of a fluorescently tagged construct³. Specifically, we have found

the iNo scores computed from the signal obtained with fluorescently tagged FBL (which labels the DFC) to be remarkably consistent with those calculated from immunofluorescence data obtained with an antibody specific to the ribosome assembly factor pescadillo³, a nucleolar protein accumulating in the GC. Hence, at least in the case of the protein depletions studied thus far, one can equally use either a DFC or a GC marker to assess nucleolar disruption³. We discuss possible alternative labeling methods for patient cells in the ‘Limitations’ section.

It has long been suspected that the nucleolus might provide a target for cancer therapy¹⁸. This hypothesis found corroboration recently, when it was demonstrated that RNA Pol I inhibitors preferentially kill cancer cells^{19,20}. Although our initial high-throughput screens were based on siRNA-mediated protein depletion, our experimental setup is directly amenable to screening compounds such as FDA-approved drugs, libraries of small molecules, or natural anticancer agents. In principle, such screens could lead to the identification of novel Pol I inhibitors, as inhibition of Pol I function produces a readily recognizable visual readout known as nucleolar segregation or ‘nucleolar caps’, which often look like ‘Mickey Mouse ears’ (Fig. 2c, see POLR1B and DDB1 panels).

Promoting the use of the iNo score seems particularly important in the context of the recent advancement of our understanding of ribosomopathies^{21–24}; as such syndromes are often associated with nucleolar alterations of varying severity. Ribosomopathies are syndromes caused by ribosome biogenesis dysfunction due to a mutation in either a ribosome assembly factor (protein or RNA) or an r-protein. Notably, ribosomopathies are often associated with cancer predisposition, although exceptions do exist, such as Treacher Collins syndrome, which is known not to be associated with cancer predisposition.

Comparison with other approaches

To our knowledge, no attempt has been made elsewhere to precisely rank nucleolar disruption by scoring the severity of alterations in cells. By providing a graded classification of structural nucleolar defects, our protocol makes it possible to compare systematically the involvement of different factors in nucleolar structure maintenance (basic cell biology research) and to compare nucleolar structure under different conditions (e.g., in health and disease in clinical research). Although other methods of nucleolar detection have been described, they are not qualitative—in the sense that they do not enable experimenters to group factors according to the ‘pattern’ of nucleolar disruption they induce once they are depleted—so these methods do not provide the means to predict the effect that they will have on the nucleolus. The unique features of our protocol are its image processing pipeline and the use of a parametric equation to determine a statistically validated mathematical score of nucleolar disruption, the iNo score. To our knowledge, this is the first time that the nucleolus has been defined both qualitatively and quantitatively in such a manner.

One alternative approach is classical AgNOR staining, which labels argyrophilic nucleolar proteins^{25,26}, including the abundant RNA Pol I transcription factor UBTF (see Mais et al.²⁷ and references therein). In AgNOR, ‘Ag’ stands for the element silver, which is used for staining, and ‘NOR’ for nucleolar organizer regions, which consist of the short arms of the five acrocentric chromosomes, where multiple copies of the rDNA are located and where the nucleoli reassemble at the end of mitosis. The AgNOR reaction is somewhat similar to silver-based photography, in that it relies on incubation of cells or tissues with gelatin and silver nitrate. AgNOR staining can be performed on formalin-fixed, paraffin-embedded biological samples²⁸. A disadvantage of this approach is that the results vary greatly according to the staining conditions used (e.g., pH, incubation time), making it difficult to use the method in routine applications such as clinical biology²⁹. Argyrophilic detection in the nucleolus can therefore reliably establish only the number of nucleoli per cell and, with precautions, the surface area of the nucleoli. Any information associated with the shape or textural features of the nucleolus is lost as a consequence of silver nitrate deposition. The applications of AgNOR staining in tumor pathology are comprehensively reviewed in Derenzini et al.⁴.

Other semiquantitative techniques consist of either counting the number of nucleoli per cell or computing the nucleolar circumference or area (e.g., Belin et al.³⁰). For example, in a study addressing the effect of stress (heat shock) on nucleolar structure, commercial software (MetaMorph) was used to measure the intensity of nucleolar pixels and the nucleolar area³¹.

In the field of digital pathology, a computer-based automated nucleolus pattern detector was developed for H&E-stained images of prostatic adenocarcinoma³². This approach aimed to present the pathologist with the most relevant biopsy sections—that is, with a selection of cells likely to

present ‘prominent’ (enlarged and supposedly malignant) nucleoli—for manual validation³². This method does not, however, allow fine stratification of nucleolar disruption.

In conclusion, the main advantage of our approach over the others is that it exploits more than just nucleolar size or intensity, or the number of nucleoli per cell nucleus; in fact, it integrates what we have established as the five most discriminant shape and textural features of the nucleolus, providing a reliable index and making it possible both to rank the severity of nucleolar disruption (the quantitative aspect or iNo score) and to distinguish phenotypic classes having predictive values (the qualitative aspect or PCA; see Anticipated results).

Experimental design

Controls

We recommend that a calibration set consisting of positive and negative controls be present in each screening plate (Fig. 2b). The controls serve to calibrate the experiment to different types of nucleolar phenotypes that one may obtain after depleting a factor of interest, namely, (i) unperturbed nucleolar morphology, (ii) fluorescence intensity decrease, (iii) more or less severe nucleolar disruption, and (iv) nucleolar segregation, also known as ‘nucleolar caps’, which are known to result from RNA Pol I inhibition⁸. The controls are important for interpretation of the PCA analysis (Fig. 2a and Anticipated results), and, in addition, they technically validate the efficiency of the siRNA-mediated depletions. The controls are as follows: for monitoring unperturbed nucleolar morphology, cells can be treated with either a nontargeting SCR siRNA or with the transfection reagent alone (no siRNA, mock); for monitoring a major fluorescence intensity decrease, cells can be treated with either an siRNA against GFP or one against FBL; for monitoring graded nucleolar disruption, cells can be treated with an siRNA against nucleolin (NCL) (NCL depletion induces moderate nucleolar disruption) or nucleophosmin (NPM) (NPM1 knockdown leads to a severe nucleolar disruption); and, finally, for monitoring nucleolar segregation, cells can be treated with an siRNA against the transcription initiation factor TIF-1A. Alternative controls include the use of chemical compounds known to affect nucleolar structure, such as actinomycin D or 5,6-dichlorobenzimidazole 1- β -D-ribofuranoside (DRB). Note that siRNAs targeting the mRNA transcripts encoding the r-proteins uL5 or uL18 can also be used, as their depletion consistently induces strong nucleolar alterations (see Anticipated results and Fig. 2c and e).

Recipient cell lines

Any cell line that can be manipulated to make it produce a fluorescently tagged nucleolar protein or that is compatible with immunofluorescence detection of a nucleolar protein can be used in this assay. To engineer a cell line expressing a fluorescent nucleolar protein, one can use standard stable transfection or CRISPR–Cas9 genome editing protocols; we have successfully used both techniques. For example, in our original large-scale siRNA screens, we used HeLa cells³, whereas for secondary screens applied to selected candidate proteins, we used other cell lines, including HCT116, MCF7, A549, and H1944. We found the impact of factor depletion on nucleolar structure to be highly similar in all the cell lines we used³.

Nucleolar subcompartment monitoring

Any of the three nucleolar subcompartments (FC, DFC, or GC) can be used in this assay, providing that a specific reporter protein can be produced or a specific antibody used. For example, as a reporter of nucleolar morphology, we initially used the box-C/D-snoRNA-associated methyltransferase FBL, which labels the DFC. In follow-up experiments, we used the pescadillo protein (PES1), which labels the GC component. We found the iNo scores computed with FBL and pescadillo to be remarkably consistent³.

Time course of siRNA-mediated factor depletion

To efficiently monitor potential defects in nucleolar morphology, it is important that cells undergo two rounds of mitosis, corresponding to two rounds of nucleolar disassembly–reassembly, and that factors be sufficiently depleted. For example, in our large-scale screens, we used 3-d siRNA-mediated depletion, reasoning that the nucleolus disassembles and reassembles at every mitosis (approximately every 24 h for routinely used cell lines—this needs to be adapted to your cell line) and that two rounds of nucleologenesis might be necessary to score morphological defects. This assumption was confirmed when we performed a time-course analysis capturing the iNo scores after 1, 2, and 3 d of

depletion of selected proteins: we observed a steady increase in the iNo score in the course of depletion and concluded that 3 d is the most suitable depletion time for scoring nucleolar alterations³.

Monitoring the efficiency of siRNA-mediated depletion

It is essential to establish the efficiency of siRNA-mediated depletion, in particular with respect to factors whose depletion does not lead to nucleolar alteration. This can be achieved by Western blotting, if suitable antibodies are available, or by RTqPCR (ref. ³³). To circumvent potential problems associated with inefficient siRNAs, we recommend systematic use of three siRNAs per target in three independent experiments³. In the example shown in Fig. 2, we used a set of siRNAs designed and validated in a previous study when we conducted high-throughput screening aimed at the identification of novel pre-rRNA processing factors³⁴. For these knockdowns, we established the efficiency of siRNA-mediated depletions in a shotgun RTqPCR analysis. Typically, we recommend testing at least 10% of all inactivations by RTqPCR.

Choice of image capture software

Any image capture software can be used. We chose to work with MetaMorph because it allows integration of hardware elements from different suppliers, and we had assembled a custom screening platform with high-end parts from different suppliers. However, 'ready-to-use' solutions are available from manufacturers that provide their own capture software (e.g., Operetta from PerkinElmer).

Use of robotics

Please note that although the use of a robot is ideal for preparing the screening plates (any liquid-handling robot will work), the plates can easily be prepared by hand using multiwell pipettes. Several plates can be prepared in parallel. An automatic cell feeder may also be used to inoculate the plates (e.g., Hamilton MicroLab STAR). If robotics is available, we recommend using the 384-well format and downscaling all steps to save expensive reagents (siRNAs, transfection reagents) and dramatically increase throughput.

Image acquisition

The input data consist of sets of images, each containing multiple nucleoli. Each image corresponds to a spatial region or site within a well in a microtiter plate. Each image includes multiple cells and gives access to a population of similarly treated nucleoli. Each site is observed at two wavelengths at least, one chosen to observe the fluorescence emitted by DAPI (the nuclear marker) and one to observe that emitted by GFP (the nucleolar marker). The DAPI channel allows individual nuclei to be segmented, whereas the GFP channel is used to characterize nucleolar phenotypes. A third channel (e.g., red fluorescence) can be used in case two nucleolar antigens are simultaneously monitored.

Image processing, segmentation, feature extraction, statistical analysis, and iNo score computation

Our computer program is organized as a main script with four subscripts. The four subscripts will successively (i) segment the images, (ii) extract the image features, (iii) compute the discrepancy vectors, and (iv) compute the iNo score and PCA. The four scripts were designed to be used sequentially.

Testing the role of noncoding RNAs on nucleolar structure

Although our protocol was initially developed to test the involvement of protein factors in nucleolar structure, it could easily be adapted to test the involvement of noncoding RNAs (ncRNAs). In this case, cells could be depleted of certain ncRNAs through the use of antisense interfering RNAs, such as gapmers and antisense oligonucleotides³⁵.

Multiplexing for monitoring the distribution of several nucleolar antigens at once

A future development of our method will be multiplexing. By combining dedicated fluorescent constructs or suitable antibodies, it will be possible to exploit multiple screening colors, for example, to monitor alterations simultaneously in the three internal layers of the nucleolus. Finally, our approach should be fully applicable to live-cell imaging screens.

Level of expertise

The researchers most likely to implement this protocol and benefit from it are cell biologists, cancer biologists, pathologists, and clinicians. This protocol can be implemented by technicians, graduate students, or post-doctoral students active in academic or clinical research environments, provided that access to a cell culture facility is granted and suitable microscopy equipment is available. All steps can be performed by one person.

Limitations

A limitation of our method is that it requires stable labeling of the nucleolus with a fluorescent marker. We have also successfully performed classic immunofluorescence detection with a specific antibody raised against a nucleolar protein. Other potential alternatives include the use of a bulk nucleolar stain such as SYTO RNaselect fluorescent stain (Thermo Fisher Scientific). Fluorescent peptides fused to nucleolar signals could also be used.

Materials

Biological materials

- Stable HeLa cell line expressing FBL tagged with GFP or an equivalent. **▲ CRITICAL** The cell line can be prepared by stable transfection of a plasmid expressing FBL–GFP or by CRISPR–Cas9 genome editing. Note that it is conceivable to use a cell line stably expressing several nucleolar markers, each epitope tagged with a compatible fluorescent protein, for example, a marker of DFC in green and a marker of GC in red (Experimental design).
- A549 (ATCC, cat. no. CRM-CCL-185), H1944 (ATCC, cat. no. CRL-5907), HeLa (ATCC, cat. no. CRM-CCL-2), and HCT116 (ATCC, cat. no. CCL-247) cells **!CAUTION** The cell lines used in your research should be regularly checked to ensure they are authentic and are not infected with mycoplasma. **!CAUTION** When initiating a new project, we strongly recommend having all the cell lines authenticated (genotyped) by short tandem repeat (STR) profiling by ATCC.

Reagents

- Absolute ethanol ($\text{CH}_3\text{CH}_2\text{OH}$; VWR, cat. no. 20821-330)
- Anti-Pes1 antibody (Invitrogen, cat. no. PA5-64020; Atlas Antibodies, cat. no. HPA040210)
- BSA (Roche, cat. no. 10735086001)
- DAPI (Sigma-Aldrich, cat. no. D9542)
- Ethylenediaminetetraacetic acid disodium salt (EDTA; Sigma-Aldrich, cat. no. E5134)
- FBS (A&E Scientific, cat. no. FBS-12A)
- Formaldehyde solution (37% (wt/vol); Sigma-Aldrich, cat. no. F8775) **!CAUTION** This reagent is toxic to eyes and skin; it may cause cancer when inhaled.
- Dulbecco's Modified Eagle's Medium high glucose with UltraGlutamine (DMEM; Lonza, cat. no. BE12-604F)
- Goat anti-rat Alexa Fluor 568 (Thermo Fisher Scientific, cat. no. A11077)
- INTERFERin siRNA transfection reagent (Polyplus-transfection, cat. no. 409-50)
- Opti-MEM I reduced-serum medium (Thermo Fisher Scientific, cat. no. 31985062)
- Penicillin–streptomycin (10,000 U/ml; Life Technologies, cat. no. 15140122)
- Potassium chloride (KCl; Sigma Aldrich, cat. no. P9333)
- Potassium phosphate monobasic (KH_2PO_4 ; Sigma-Aldrich, cat. no. P0662)
- siRNAs, 100 nM (Silencer Select siRNAs; Life Technologies)
- Sodium chloride (NaCl; Sigma-Aldrich, cat. no. S3014)
- Sodium phosphate, dibasic (Na_2HPO_4 ; Sigma-Aldrich, cat. no. S7907)
- Triton X-100 (MP Biomedicals, cat. no. 807426) **!CAUTION** Triton X-100 is an irritant to skin and eyes, and is hazardous to the environment.
- HCl 10 N/37% (wt/vol) (VWR, cat. no. 20252.295)
- NaOH (Sigma-Aldrich, cat. no. S8045)
- Trypsin–EDTA solution (Westburg-Lonza, cat. no. LO BE17-161E) **!CAUTION** This solution should be used only in cases in which the cells do not detach well in 1× PBS (pH 7.4/0.5 mM) EDTA.
- Muse Count & Viability Assay Kit (Millipore, cat. no. MCH100102)

Equipment

- Automatic pipettes of 0.1–1,000- μ l volume
- Automatic multichannel pipette, 100- μ l volume
- Culture chamber with 95% humidified atmosphere containing 5% CO₂ and set to 37 °C
- 20 \times /0.5 objective lens (Zeiss; EC Plan-Neofluar) (for screening)
- 100 \times /1.46 α Plan-Apochromat objective lens (for high-resolution imaging)
- Freezer (–20 °C)
- CCD camera (Roper, model no. HQ2 Coolsnap)
- Autofocus device (Zeiss Definite Focus.2)
- Laminar-flow biosafety cabinet
- MetaMorph: Meta Series Software v.7.7.0–7.10.1 (MDS Analytical Technologies, <https://www.moleculardevices.com/products/cellular-imaging-systems/acquisition-and-analysis-software/metamorph-microscopy>)
- Neubauer hemocytometer
- Petri dishes (10 cm²)
- Pipette tips
- Refrigerator
- Sterile polypropylene conical tubes, 15- and 50-ml volume
- Water bath (37 °C)
- 96-Well black glass-bottom plates with lids, individually packed and sterile (Corning, cat. no. 324002)
- Adhesive multiwell sealing film (MicroAmp optical adhesive film; Thermo Fisher, cat. no. 4311971)
- (Optional) Automatic cell feeder (e.g., Hamilton MicroLab STAR)
- Inverted microscope to monitor cell culture
- Muse cell analyzer (Merck)
- We use an automated high-throughput screening microscopy platform driven by MetaMorph, consisting of a Zeiss Axio Observer Z1 microscope equipped with a motorized stage (Princeton Instruments), a cool LED excitation system, a CCD camera (HQ2 Coolsnap, Roper), and a Zeiss 20 \times EC Plan-Neofluar objective (0.5 numerical aperture). **▲ CRITICAL** ‘Ready-to-use’ alternative solutions are available from companies such as Molecular Devices (ImageXpress), GE Healthcare Life Sciences (IN Cell Analyzer, model no. 6500HS), PerkinElmer (Operetta CLS), or Nikon Instruments (HC High Content Analysis System).
- MATLAB software with ‘Image Processing’ and ‘Statistics Toolboxes’, available from <https://www.mathworks.com/products/matlab.html>.
- Computer. There are no particular hardware requirements, although we recommend working on independent workstations for the image capture and image processing analysis. The following system was used for all analyses performed in our laboratory using this protocol: Ubuntu desktop 14.04, Intel® Core™2 Quad CPU Q8200 processor at 2.33 GHz \times 4.
- iNo score image-processing algorithm³: available for download at <https://github.com/LafontaineLab/iNo-score>.

Reagent setup

10 \times PBS, pH 7.4

Prepare 1 liter of solution by mixing 1.37 mol NaCl (80 g), 27 mmol KCl (2 g), 100 mmol Na₂HPO₄ (144 g), and 18 mmol KH₂PO₄ (2.4 g); adjust pH to 7.4 with 10 N HCl or 10 M NaOH; and add dH₂O up to a 1-L final volume. Then autoclave for 30 min at 120 °C. Store at room temperature (23 °C) for up to 1 year.

DMEM culture medium

Supplement 500 ml of DMEM with 10% (vol/vol) FBS and 50 U/ml penicillin–streptomycin. Store at 4 °C protected from light for up to 4 weeks. **▲ CRITICAL** Keep the ingredients sterile and prepare the solution under a cell culture hood, wearing clean gloves and after having cleaned everything with 70% (vol/vol) ethanol or any appropriate disinfectant to avoid contamination. Check for contamination (typically, a change in color, i.e., becomes turbid) each time before every use.

0.5 M EDTA stock solution, pH 8

Dissolve 46.5 g of EDTA powder in 200 ml of dH₂O. Adjust the pH to 8 with 10 N NaOH and add dH₂O to a final volume of 250 ml. Autoclave for 30 min at 120 °C and store at 4 °C for years.

▲ **CRITICAL** EDTA dissolves completely and the solution becomes transparent once the pH is adjusted.

1× PBS, pH 7.4/0.5 mM EDTA

Dilute 50 ml of 10× PBS and 0.5 ml of EDTA stock solution (0.5 M) in dH₂O (500 ml final volume). Autoclave for 30 min at 120 °C. Store at room temperature for up to 1 year.

1× PBS, pH 7.4/2% (vol/vol) formaldehyde

For a full 96-well plate, prepare (just before use) a 10-ml solution by mixing 1 ml of 10× PBS, pH 7.4, with 540 µl of 37% (wt/vol) formaldehyde and adding dH₂O to 10 ml. **! CAUTION** Formaldehyde is harmful to the eyes and skin, so the solution must be prepared in a fume hood, while wearing gloves.

2% (wt/vol) BSA

Just before use, prepare a 10-ml solution (for a full 96-well plate) by dissolving 0.2 g of BSA powder in 10 ml of 1× PBS.

0.2% (vol/vol) Triton X-100/2% (wt/vol) BSA solution

Just before use, prepare 10 ml of 2% (wt/vol) BSA and add 20 µl of Triton X-100. **! CAUTION** Triton X-100 is an irritant to the skin and eyes. Prepare the solution under a fume hood while wearing gloves.

10 N NaOH

Dissolve 40 g of NaOH pellets in 100 ml of water.

Equipment setup**Image capture**

Use any image capture software compatible with your hardware. We used MetaMorph only because it allowed integration of hardware elements from different suppliers. Set the exposure times for each of the following channels as follows: DAPI at 300 ms, GFP at 300 ms, and Red channel (Alexa Fluor 568) (if needed) at 1 s. These exposure times are only examples and should be adapted to your samples. Set the objective lens for appropriate image resolution acquisition (typically, 20× for screenings; 40× can also be used) and define a stage offset for optimal focus. Adjust the number of independent fields of view captured per well to 16.

Image processing analysis

Install the MATLAB software with the image processing and statistics toolboxes on a computer workstation.

Procedure**Reverse siRNA transfection of human cells to deplete nucleolar protein expression****● Timing ~74 h**

▲ **CRITICAL** Steps 1–12 must be performed under a sterile hood to prevent any bacterial or fungal contamination. Before use, clean all equipment (e.g., pipettes) and bottles of reagents with 70% (vol/vol) ethanol or another appropriate disinfectant.

▲ **CRITICAL** For each target, use at least three independent silencer RNAs in three individual reactions, and repeat all screens at least three times.

1 Culture a HeLa cell line stably expressing fluorescent FBL (or another nucleolar marker) for four or five passages (typically diluting them every 2–3 d) in DMEM-rich medium in a 10-cm² Petri dish at 37 °C under 5% CO₂ in a humidified incubator to a density of up to 10⁶ cells/ml. Gently thaw an aliquot of cells from your storage facility (liquid nitrogen tank) and use it to inoculate a Petri dish filled with fresh medium. It usually takes 24 h to revive the cells from the stocks.

▲ **CRITICAL STEP** In this step, one can either use a human cell line stably expressing a fluorescently tagged nucleolar marker (such as FBL) or cells in which a nucleolar protein will be detected by immunofluorescence. In both cases, the culture and transfection (Steps 1–8) are identical. For example, we have successfully used an anti-PES1 antibody on A549, H1944, HeLa, and HCT116 cells (Box 1).

▲ CRITICAL STEP Use low-passage cells (typically grown for five to ten passages) for your transfections; make sure the cells are growing healthily and that >90% of them are alive before transfection. A Muse cell analyzer and a Muse Count & Viability Assay Kit can be used for this purpose. Do not exceed 80% cell confluence.

? TROUBLESHOOTING

- 2 Split the cell cultures every 2–3 d. Before splitting the cells, check the cell density and for the absence of contamination under an inverted microscope. To split the cells, aspirate the culture medium, wash the cells once with prewarmed 1× PBS, pH 7.4, and then add 1 ml of prewarmed 1× PBS, pH 7.4/0.5 mM EDTA to detach the cells. Incubate the dish in a humidified chamber (37 °C, 5% CO₂) for 10 min until the cells detach (check under an inverted microscope). Resuspend the cells by pipetting gently up and down. Collect 10 μl of cell suspension and transfer this sample to the counting chamber of a Neubauer hemocytometer. Count the cells under an inverted microscope and calculate the cell concentration (*n* cells counted in the hemocytometer corresponds to a concentration of $n \times 10^4$ cells/ml). Dilute the cells with DMEM culture medium to a concentration of 5,000 cells per well of a 96-well plate (or 7×10^4 cells/ml). Keep the cell suspension in a flask in a humidified chamber (37 °C, 5% CO₂) until you need it in Step 7.

▲ CRITICAL STEP Use a water bath at 37 °C to prewarm the above-mentioned solutions.

▲ CRITICAL STEP Alternatively, if the cells do not detach easily using 1× PBS, pH 7.4/0.5 mM EDTA, use a trypsin–EDTA solution instead.

▲ CRITICAL STEP It is not necessary to monitor the level of humidity in the incubator to perform these cultures; however, make sure that the water pan at the bottom of the incubator is well filled with water at all times.

▲ CRITICAL STEP The cell suspension should not be maintained for >1 h. You must use the cells as soon as possible.

- 3 Mix together 12.5 μl of INTERFERin and 2 ml of Opti-MEM medium.

▲ CRITICAL STEP This step is performed to obtain mixtures to be transferred to each well of a 96-well plate while achieving the best pipetting accuracy for preparing a large volume (enough mix for 100 wells, in this case).

- 4 Incubate the mixture for 10 min at room temperature and then pipette 20-μl aliquots of it into each well of a 96-well plate. Vortex the plate for 5 s.

▲ CRITICAL STEP If many wells are to be used, use a multichannel pipette to reduce the time needed.

- 5 Add a 10-μl aliquot of the desired siRNA solution (10 nM final concentration, prepared from a 100 nM siRNA stock) to each well of the 96-well plate and mix gently by pipetting up and down. In each plate, make sure to set up a series of positive and negative controls (Experimental design and Fig. 2b).

▲ CRITICAL STEP For each target, three individual siRNAs are to be used (i.e., three wells per target gene) and three independent experiments (replicates) (i.e., three screening 96-well plates) should be set up.

▲ CRITICAL STEP As long as the siRNA solutions are in use, keep them on ice to avoid spontaneous RNA degradation. Always store siRNA solutions at –20 °C (100 nM stocks remain stable for several years; discard diluted solutions) and make aliquots to avoid repeated freeze–thaw cycles that may also cause siRNA degradation.

- 6 Incubate the 96-well plate for 20 min at room temperature.

- 7 Add 70 μl of the cell suspension prepared in Step 2 to each well and mix gently by pipetting up and down. The final volume per well is 100 μl.

- 8 Incubate the 96-well plate for 72 h in a humidified chamber (37 °C, 5% CO₂)

▲ CRITICAL STEP 72 h of incubation time for the siRNA-mediated depletion of target genes is considered ideal, as discussed further in the ‘Experimental design’ section.

? TROUBLESHOOTING

Cell fixation and preparation for microscope scanning ● Timing 20 min for a 96-well plate

- 9 Remove the culture medium from each well with a multichannel pipette and fix the cells by adding 100 μl of 2% (wt/vol) formaldehyde/1× PBS buffer to each well.

▲ CRITICAL STEP Avoid vacuum aspiration of the culture medium and buffers; make sure to perform manual aspiration to prevent loss of cells from the plate.

- 10 Incubate the 96-well plate for 15 min at room temperature.

- 11 Wash the plate three times with 1× PBS.

DAPI staining of HeLa cells expressing fluorescent FBL protein ● Timing 35 min for a 96-well plate

- 12 Add 100 μ l of freshly made 100 ng/ml DAPI solution to each well. Alternatively, if you are using immunofluorescence staining of nucleolar marker protein(s) rather than cell lines expressing fluorescently tagged proteins, follow the procedure in Box 1 before continuing with this step.
- 13 Incubate the 96-well plate for 15 min at room temperature.
- 14 Wash the plate three times with 1 \times PBS (5 min each time).
- 15 Add 100 μ l of 1 \times PBS to each well.
- 16 To avoid desiccation, seal the plate with a dedicated adhesive multiwell sealing film and cover it with the plate lid.
- 17 Wrap the sealed plate with aluminum foil to protect it from light and store at 4 $^{\circ}$ C.
▲ CRITICAL STEP Although it is better to image the plates immediately, we have found the fluorescent signals to be extremely stable and the cell morphology to be well preserved. The plates can thus be imaged for several weeks, or even for several months, with similar results. This behavior is very convenient for confirmatory purposes, when one wishes to image particular wells a second time (e.g., in case of insufficient sampling or focus problems) or simply for imaging plates at remote facilities.

Image acquisition ● Timing 3 h for a 96-well plate

- 18 Remove the plate lid and place the plate on the stage platform of the microscope (with an inset for 96-well plates).
▲ CRITICAL STEP The plates can be placed onto the microscope stage manually, or a robotic arm can be installed to increase throughput.
- 19 Switch on the camera, the computer, and the wide-field fluorescence mode of the microscope, and start MetaMorph.
- 20 Use an EC Plan-Neofluar 20 \times , 0.5 numerical aperture objective lens.
- 21 Select ‘plate acquisition setup’ in the MetaMorph program and select 16 sites to be acquired per well.
- 22 Select the desired wavelengths for DAPI (358 nm excitation/463 nm emission) and GFP (489 nm excitation/509 nm emission), and set the initial exposure time for both at 300 ms.
▲ CRITICAL STEP If immunofluorescence staining involves the use of red fluorescence detection, select a third channel as required (for Alexa Fluor 568: 576 nm excitation/603 nm emission) and set the initial exposure time to 1 s for this channel.
- 23 Manually adjust the *z*-axis position to find the optimal focal position of the microscope.
- 24 Take a snapshot before starting to scan the whole plate to make sure that the image acquired has the highest possible resolution and focus.
? TROUBLESHOOTING
- 25 Start your image capture software’s automated acquisition script (here, MetaMorph).
- 26 Save the images as 16-bit TIFFs on the hard drive of the computer.
▲ CRITICAL STEP Turn off the light in the room to avoid photobleaching of the fluorochrome. After scanning, you can store the plates again at 4 $^{\circ}$ C for up to several months (Step 17). It is possible to scan them again later should the need arise (because of focus problems or insufficient sampling, or in the case that the plates are prepared and imaged at different facilities).
? TROUBLESHOOTING

Image processing and statistical analysis: predictive functional clustering (PCA) and iNo score computation ● Timing 16 h for a 96-well plate

- ▲ CRITICAL** In Step 27, instructions are provided to run the overall script that performs the functions needed to carry out image processing, image segmentation, feature extraction, statistical analysis, iNo score determination, and factor ranking. All these steps are performed in MATLAB. The overall script, however, comprises four individual ‘mandatory’ subscripts, which were designed to be used in sequence (Box 2).
- ▲ CRITICAL** In particular circumstances, it may be necessary to adapt the morphometric feature parameters to the data at hand. To achieve this goal, run the script ‘s_optimize_parameters.m’ (Box 2). Use of this script is optional, and the conditions in which we recommend that it be implemented are described in Box 2.
- 27 Download and extract the image processing pipeline from the software archive (available at <https://github.com/LafontaineLab/iNo-score>) and open it with MATLAB.

- 28 To analyze your images statistically (by PCA) and compute the iNo scores, copy your image dataset (from Step 26) into the 'data' repository (automatically created once the software archive has been installed). Create one subrepository for each multiwell plate. The names of the images should be either X_Y_sZ_dapi.TIF (DAPI image) or X_Y_sZ_gfp.TIF (FIB_GFP image), where X is the name of the plate subrepository, Y refers to the index of the well, and Z is the index of the image site in the well. For example, data/plate2/plate2_B09_s14_dapi.TIF refers to the 14th DAPI image of well B09 of plate number 2.
- 29 Create a 'dataconfig.m' file in the 'data' directory, using the command `struct('plate', X, 'well', Y, 'gene_name', G, 'gene_index', 0);` (where X, Y, and G denote the name of the plate subdirectory, the index of the well, and the name of the depleted protein of interest, respectively).
 This file defines the number of sites per well. It also defines the protein of interest that has been depleted in each well. In practice, the protein of interest is chosen from among those defined in the 'gene_name' variable (e.g., 'uL5' or 'SCR').
- 30 Run the script 's_main.m' in MATLAB so as to segment the nuclei, compute their features, and analyze them.
▲ CRITICAL STEP This script automatically runs four subscripts that are described in more detail in Box 2 and that can be started independently in a sequence if desired.
▲ CRITICAL STEP For improved computational efficiency, the segmentation of multiple images can be done in parallel, as can the computation of all the various morphometric features. The use of a cluster will speed up the process.

Troubleshooting

Troubleshooting advice can be found in Table 1.

Step	Problem	Possible reason	Solution
1	Incorrect cell density	Incorrect or ineffective seeding	Establish a precise cell count before dilution, using a hemocytometer, and allow cells to reach 80% cell confluency before transfection
8		Cell toxicity after siRNA-mediated depletion	Decrease the depletion time (<72 h)
24	Image quality is low	Image is out of focus	Program a suitable offset with respect to the bottom of the plate by using an autofocus device such as the Zeiss Definite Focus. Alternatively, establish the focus by capturing a z stack at first acquisition
		Image background is high	Optimize fluorescent dye concentration (either that of DAPI or of the secondary fluorescent antibodies, in the case of immunofluorescence) or wash with PBS for longer periods of time to remove unbound fluorophores
		Photobleaching	Minimize sample exposure to light
		Uneven illumination	The light path of the microscope needs to be aligned
26	Images are totally black	Image formatting is incorrect	Convert the images to RGB format with an appropriate program (e.g., ImageJ (https://imagej.nih.gov/ij/))
Box 2, step 1	The image is over- or undersegmented (segmentation is acceptable when the software identifies one nucleus per cell and when the nucleolar masses are precisely counterstained by the DNA stain)	The image is weakly contrasted	Reacquire the image or exclude it from consideration in the analysis
	The number of cells imaged per well is too small (<200)	In the field of view used, the number of cells was insufficient	Acquire new images of that well. To achieve statistical relevance, ≥200 cells should be captured
Box 2, step 4	The PCA analysis is not relevant. The software automatically determines whether the PCA analysis is statistically relevant. If it is not, an error message is displayed to let the experimenter know	The number of wells analyzed is insufficient (<10)	Repeat the analysis with >10 wells (if the number of wells is <10, then the PCA analysis is not relevant)

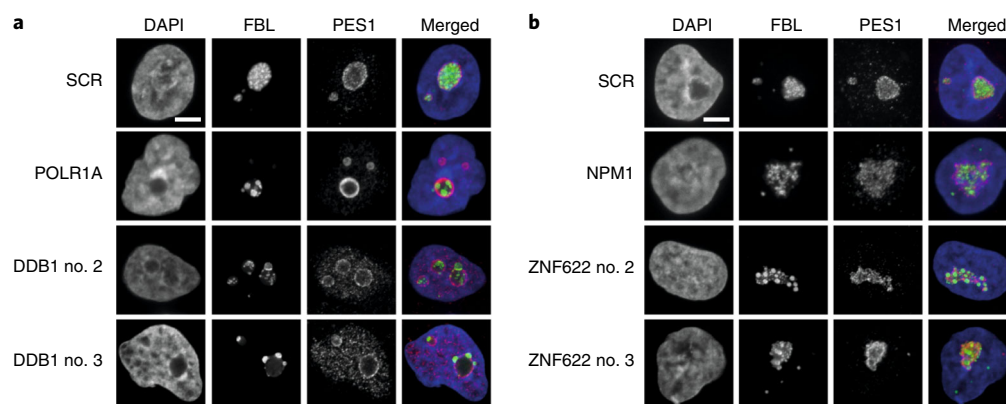


Fig. 3 | Examples of validation of nucleolar morphological alterations by high-resolution imaging. a,b, To confirm the role of DDB1 (**a**) and ZNF622 (**b**) in nucleolar structure maintenance, HeLa cells separately depleted of each protein were imaged by spinning-disk confocal microscopy at 100× magnification. As controls, cells were treated with a nontargeting scramble (SCR) siRNA, or an siRNA specific to transcripts encoding a subunit of RNA Pol I (POLR1A) or nucleophosmin (NPM1). Cells expressing green fluorescent FBL, which labels the DFC compartment of the nucleolus, were stained with DAPI (to label the DNA) and with an anti-PES1 antibody (to detect the GC). For DDB1 and ZNF622 depletion, three independent siRNAs were used; for simplicity, results obtained with two siRNAs (nos. 2 and 3) are shown. DDB1 depletion leads to formation of nucleolar caps (nucleolar segregation), as is typically seen after POLR1A depletion. Depletion of ZNF622 leads to a major and unique nucleolar structure alteration, in which fibrillarin forms regularly spaced and similarly sized foci throughout the entire nucleolar volume; a phenotype that, to our knowledge, has never before been documented. Scale bars, 5 μm .

Timing

Steps 1–7, reverse siRNA transfection of human cells to deplete nucleolar protein expression: ~2 h

Step 8, incubation of cells: 72 h

Steps 9–11, cell fixation and preparation for microscope scanning: 20 min per plate

Steps 12–17, DAPI staining of HeLa cells expressing fluorescent FBL protein: 35 min per plate

Steps 18–26, image acquisition: 3 h per plate

Steps 27–30, image processing and statistical analysis: 16 h per plate

Box 1, immunofluorescence staining of a human cell line for the detection of one (e.g. PES1) or several nucleolar proteins, 5 h 30 min per plate

Box 2, the execution time depends on the number of nuclei per image. The following values correspond to the mean execution time for an image site including 200 nuclei on an i7-4600U 2.1-GHz processor with 16 Gb RAM: step 1, segmentation: 30 s per image; step 2, computation of the five features: 4 s per image; step 3, computation of the discrepancy vectors: negligible (~0.5 s for 16 wells, each well corresponding to 16 images); step 4, iNo computation and PCA analysis: negligible

Anticipated results

This protocol can be used to explore a number of different research questions, so, to provide readers with information on the kinds of results they may expect to obtain after implementing the Procedure, we detail below a few example applications of the protocol carried out in our laboratory.

Typically, the Procedure will allow factors to be ranked with respect to their requirement for nucleolar structure maintenance (i.e., according to the severity of nucleolar disruption observed after their depletion); in some cases, it will allow the function of uncharacterized factors in the nucleolar structure and ribosome biogenesis to be predicted.

The Procedure allows both quantitative and qualitative analysis. A typical quantitative analysis, or iNo score ranking, is shown in Fig. 2e. The iNo score ranges from 0 (factor depletion has no effect on nucleolar structure) to 0.25 (factor depletion very severely impacts nucleolar structure). The iNo score is used to grade nucleolar disruption.

A typical qualitative analysis, or PCA, is shown in Fig. 2a. Each symbol represents a population of >200 cells in which a factor has been depleted with one siRNA specific to one cellular target. The graph shows that (i) the vast majority of proteins tested do not greatly impact nucleolar structure, as in the case of gene products appearing in the vicinity of the reference controls (notably, close to the SCR and MOCK controls), (ii) a few proteins impact nucleolar structure severely, as in the case of

proteins at the periphery of the graph, and these are grouped according to the pattern of nucleolar disruption they induce once they are depleted (e.g., uL5 and uL18 to the right, and TIF1A and POLR1B to the left; UTP-A components also cluster with TIF1A and POLR1B, see below and Figs. 2d and 3), and (iii) identical symbols are often close to each other; these represent different siRNAs against the same target, and their proximity on the graph demonstrates the robustness of the Procedure (i.e., depleting a protein using different siRNAs produces the same or a similar pattern of nucleolar disruption). The pattern of nucleolar disruption observed upon depletion of a factor of interest may reflect its function. For example, TIF1A and POLR1B are both involved in pre-rRNA synthesis; their depletion induces the formation of typical nucleolar caps, and the two proteins are quite close on the PCA graph. Also illustrated are the nucleolar caps observed upon depletion of other ribosome assembly factors important for pre-rRNA synthesis (UTP-A components of the small subunit (SSU) processome, Fig. 2d), which strikingly all cluster spatially with POLR1B and TIF1A on the PCA plot (Fig. 2a). Similarly, r-proteins uL5 and uL18 are part of the same structure on the ribosome (the central protuberance, see below); they are assembled at the same time onto the maturing large ribosomal subunit, and their depletion affects the nucleolar structure in a similar manner; thus, they are grouped together on the PCA. Remarkably, uL18 (also known as RPL5) carries four R-motifs (RX_nR, where X is any amino acid and $n \leq 2$), which interact with NPM and are important for nucleolar formation by phase transition³⁶.

As a means to further illustrate our Procedure, we will now describe in more detail two case studies performed in our laboratory:

Case study 1: r-Protein screen

Using the 80 human r-proteins as a tester set, we showed, unexpectedly, that only a few late-assembling r-proteins of the large subunit are important for nucleolar structure maintenance, whereas the rest of the r-proteins of the large subunit and those of the small subunit are dispensable³. The most important contributors to nucleolar structure turned out to be the r-proteins uL5 (formerly RPL11) and uL18 (RPL5). These two proteins, together with the 5S rRNA, form a trimeric ribonucleoprotein complex important in regulating the homeostasis of the anticancer protein p53 (ref. ³).

The importance of uL5 and uL18 is particularly interesting because it illustrates the predictive power of using the iNo score. It shows that it is possible to predict the involvement in nucleolar structure maintenance of factors that had not yet been connected to this process, such as BXDC1 and RRS1. Indeed, in the mature 60S ribosomal subunit, uL5 and uL18 form the central protuberance (CP), a late-assembling structure of the subunit essential to its overall architecture and function. In both budding yeast and human cells, several factors have been shown to be required for CP formation, notably BXDC1 and RRS1 (refs. ^{37,38}). Our observations with uL5 and uL18 led us to predict that inhibiting CP formation by depleting the CP assembly factors BXDC1 or RRS1 should lead to severe nucleolar structure disruption, and, indeed, this is what we confirmed (Nicolas et al.³). Remarkably, the iNo scores computed after CP assembly factor depletion were very similar to those observed after uL5 or uL18 depletion³.

Case study 2: Nucleolar protein screen

In a follow-up study, the effect on nucleolar structure of depleting the expression of 668 abundant nucleolar proteins was tested: depletion of 40% of them (273 proteins) was found to induce a nucleolar defect of sufficient importance to be visible to the experimenter's eyes. Depletion of the other 60% (395 proteins) did not impact nucleolar morphology significantly. PCA and iNo score ranking were performed for the 86 proteins whose depletion impacted nucleolar structure maintenance the most severely (Fig. 2). The analysis confirmed uL5 and uL18 as cell components essential to nucleolar structure maintenance (Fig. 2a,c,e).

The proteins DDB1 and ZNF622 attracted our attention. DDB1 because its depletion induces a very well-characterized nucleolar disruption pattern known as 'nucleolar segregation' or 'nucleolar caps', typically associated with loss of RNA Pol I function⁸ (Fig. 2c, compare POLR1B and DDB1 panels, and Fig. 3a, compare the POLR1A and DDB1 panels; POLR1A and POLR1B are two subunits of RNA Pol I) and ZNF622, a factor involved in late assembly of the large ribosomal subunit³⁹, because its depletion was associated with a remarkable nucleolar disruption phenotype in which FBL forms regularly spaced and similarly sized foci throughout the entire nucleolar volume (Figs. 2 and 3).

The example of DDB1 is interesting because this protein was known to be involved in DNA repair but had not previously been linked to ribosomal biogenesis or rRNA synthesis⁴⁰. Because depletion of

DDB1 led to the formation of ‘nucleolar caps’, we predicted it might be involved in pre-rRNA synthesis. This was indeed confirmed when we showed the presence of DDB1 at the rDNA locus by chromatin immunoprecipitation (V.S., P.P., C.D.V., and D.L.J.L., data not shown) and demonstrated its involvement in RNA synthesis by quantitative northern blotting and metabolic labeling (using in vivo L-[methyl-³H] methionine pulse-chase assay and click chemistry with direct microscopic visualization of fluorescently labeled pre-rRNAs; see Supplementary Fig. 1). Furthermore, severe ribosome biogenesis inhibitions are known to trigger an antitumoral surveillance pathway, leading to the stabilization of p53 (ref. ³), and we found this to be the case after depletion of DDB1 (Supplementary Fig. 1). A protocol for in vivo pulse labeling of rRNAs with bromouridine-5′-triphosphate followed by antibody detection was described⁴¹ that may also be used in follow-up studies to address the function of factors in relation to the spatial distribution of nascent transcripts.

References

1. Boulon, S., Westman, B. J., Hutten, S., Boisvert, F. M. & Lamond, A. I. The nucleolus under stress. *Mol. Cell* **40**, 216–227 (2010).
2. Boisvert, F. M., van Koningsbruggen, S., Navascues, J. & Lamond, A. I. The multifunctional nucleolus. *Nat. Rev. Mol. Cell Biol.* **8**, 574–585 (2007).
3. Nicolas, E. et al. Involvement of human ribosomal proteins in nucleolar structure and p53-dependent nucleolar stress. *Nat. Commun.* **7**, 11390 (2016).
4. Derenzini, M., Montanaro, L. & Trere, D. What the nucleolus says to a tumour pathologist. *Histopathology* **54**, 753–762 (2009).
5. Salvetti, A. & Greco, A. Viruses and the nucleolus: the fatal attraction. *Biochim. Biophys. Acta* **1842**, 840–847 (2014).
6. Buchwalter, A. & Hetzer, M. W. Nucleolar expansion and elevated protein translation in premature aging. *Nat. Commun.* **8**, 328 (2017).
7. Fulka, H., Kyogoku, H., Zatssepina, O., Langerova, A. & Fulka, J. Jr. Can nucleoli be markers of developmental potential in human zygotes? *Trends Mol. Med.* **21**, 663–672 (2015).
8. Hernandez-Verdun, D., Roussel, P., Thiry, M., Sirri, V. & Lafontaine, D. L. J. The nucleolus: structure/function relationship in RNA metabolism. *Wiley Interdiscip. Rev. RNA* **1**, 415–431 (2010).
9. Lafontaine, D., De Vleeschouwer, C., Nicolas, E. & Parisot, P. Nucleolar structure evaluation and manipulation. European patent WO2017191187A2 (2016) (16168087.1-1408).
10. Feric, M. et al. Coexisting liquid phases underlie nucleolar subcompartments. *Cell* **165**, 1686–1697 (2016).
11. Mitrea, D. M. et al. Self-interaction of NPM1 modulates multiple mechanisms of liquid-liquid phase separation. *Nat. Commun.* **9**, 842 (2018).
12. Thiry, M. & Lafontaine, D. L. J. Birth of a nucleolus: the evolution of nucleolar compartments. *Trends Cell Biol.* **15**, 194–199 (2005).
13. Sobecki, M. et al. The cell proliferation antigen Ki-67 organises heterochromatin. *eLife* **5**, e13722 (2016).
14. Zhu, L. & Brangwynne, C. P. Nuclear bodies: the emerging biophysics of nucleoplasmic phases. *Curr. Opin. Cell Biol.* **34**, 23–30 (2015).
15. Courchaine, E. M., Lu, A. & Neugebauer, K. M. Droplet organelles? *EMBO J.* **35**, 1603–1612 (2016).
16. Shin, Y. & Brangwynne, C. P. Liquid phase condensation in cell physiology and disease. *Science* **357**, eaaf4382 (2017).
17. Weber, S. C. & Brangwynne, C. P. Inverse size scaling of the nucleolus by a concentration-dependent phase transition. *Curr. Biol.* **25**, 641–646 (2015).
18. Drygin, D., Rice, W. G. & Grummt, I. The RNA polymerase I transcription machinery: an emerging target for the treatment of cancer. *Annu. Rev. Pharmacol. Toxicol.* **50**, 131–156 (2010).
19. Bywater, M. J. et al. Inhibition of RNA polymerase I as a therapeutic strategy to promote cancer-specific activation of p53. *Cancer Cell* **22**, 51–65 (2012).
20. Peltonen, K. et al. A targeting modality for destruction of RNA polymerase I that possesses anticancer activity. *Cancer Cell* **25**, 77–90 (2014).
21. McCann, K. L. & Baserga, S. J. Genetics. Mysterious ribosomopathies. *Science* **341**, 849–850 (2013).
22. Narla, A. & Ebert, B. L. Translational medicine: ribosomopathies. *Blood* **118**, 4300–4301 (2011).
23. De Keersmaecker, K., Sulima, S. O. & Dinman, J. D. Ribosomopathies and the paradox of cellular hypo- to hyperproliferation. *Blood* **125**, 1377–1382 (2015).
24. Yelick, P. C. & Trainor, P. A. Ribosomopathies: global process, tissue specific defects. *Rare Dis.* **3**, e1025185 (2015).
25. Ploton, D. et al. Improvement in the staining and in the visualization of the argyrophilic proteins of the nucleolar organizer region at the optical level. *Histochem. J.* **18**, 5–14 (1986).
26. Trere, D. AgNOR staining and quantification. *Micron* **31**, 127–131 (2000).
27. Mais, C., Wright, J. E., Prieto, J. L., Raggett, S. L. & McStay, B. UBF-binding site arrays form pseudo-NORs and sequester the RNA polymerase I transcription machinery. *Genes Dev.* **19**, 50–64 (2005).
28. Derenzini, M. & Ploton, D. Interphase nucleolar organizer regions in cancer cells. *Int. Rev. Exp. Pathol.* **32**, 149–192 (1991).

29. Aubele, M. et al. Guidelines of AgNOR quantitation. Committee on AgNOR quantitation within the European Society of Pathology. *Zentralbl. Pathol.* **140**, 107–108 (1994).
30. Belin, S. et al. Dysregulation of ribosome biogenesis and translational capacity is associated with tumor progression of human breast cancer cells. *PLoS ONE* **4**, e7147 (2009).
31. Kодиha, M., Banski, P. & Stochaj, U. Computer-based fluorescence quantification: a novel approach to study nucleolar biology. *BMC Cell Biol.* **12**, 25 (2011).
32. Yap, C. K. et al. Automated image based prominent nucleoli detection. *J. Pathol. Inform.* **6**, 39 (2015).
33. Green, M. R. & Sambrook, J. *Molecular Cloning: A Laboratory Manual* 4th edn (Cold Spring Harbor Laboratory Press, Cold Spring Harbor, NY, 2012).
34. Tafforeau, L. et al. The complexity of human ribosome biogenesis revealed by systematic nucleolar screening of pre-rRNA processing factors. *Mol. Cell* **51**, 539–551 (2013).
35. Ideue, T., Hino, K., Kitao, S., Yokoi, T. & Hirose, T. Efficient oligonucleotide-mediated degradation of nuclear noncoding RNAs in mammalian cultured cells. *RNA* **15**, 1578–1587 (2009).
36. Mitrea, D. M. et al. Nucleophosmin integrates within the nucleolus via multi-modal interactions with proteins displaying R-rich linear motifs and rRNA. *eLife* **5**, e13571 (2016).
37. Sloan, K. E., Bohnsack, M. T. & Watkins, N. J. The 5S RNP couples p53 homeostasis to ribosome biogenesis and nucleolar stress. *Cell Rep.* **5**, 237–247 (2013).
38. Zhang, J. et al. Assembly factors Rpf2 and Rrs1 recruit 5S rRNA and ribosomal proteins rpL5 and rpL11 into nascent ribosomes. *Genes Dev.* **21**, 2580–2592 (2007).
39. Greber, B. J. et al. Insertion of the biogenesis factor Reil probes the ribosomal tunnel during 60S maturation. *Cell* **164**, 91–102 (2016).
40. Angers, S. et al. Molecular architecture and assembly of the DDB1-CUL4A ubiquitin ligase machinery. *Nature* **443**, 590–593 (2006).
41. Thiry, M. et al. A protocol for studying the kinetics of RNA within cultured cells: application to ribosomal RNA. *Nat. Protoc.* **3**, 1997–2004 (2008).

Acknowledgements

V.S. was the recipient of a fellowship from the Fonds National de la Recherche Scientifique (F.R.S./FNRS). The De Vleeschouwer lab is supported by the Fonds National de la Recherche Scientifique (F.R.S./FNRS) and the Walloon Region (DGO6). The Lafontaine lab is supported by the Université Libre de Bruxelles (ULB), the Fonds National de la Recherche Scientifique (F.R.S./FNRS), the Walloon Region (DGO6), the Fédération Wallonie-Bruxelles, and the European Research Development Fund (ERDF) through its affiliation with the Centre for Microscopy and Molecular Imaging (CMMI). The Lafontaine Lab is also affiliated with the ULB Cancer Research Center (U-CRC).

Author contributions

V.S. performed the wet lab experimental work. V.S. and D.L.J.L. interpreted the data. P.P. wrote the computer script and performed the image processing analysis. C.D.V. supervised the code production and statistical analysis. D.L.J.L. designed the project, helped with code production, and integrated the data. All authors contributed to writing the manuscript.

Competing interests

The authors declare no competing interests.

Additional information

Supplementary information is available for this paper at <https://doi.org/10.1038/s41596-018-0044-3>.

Reprints and permissions information is available at www.nature.com/reprints.

Correspondence and requests for materials should be addressed to D.L.J.L.

Publisher's note: Springer Nature remains neutral with regard to jurisdictional claims in published maps and institutional affiliations.

Published online: 24 September 2018

Related link

Key reference using this protocol

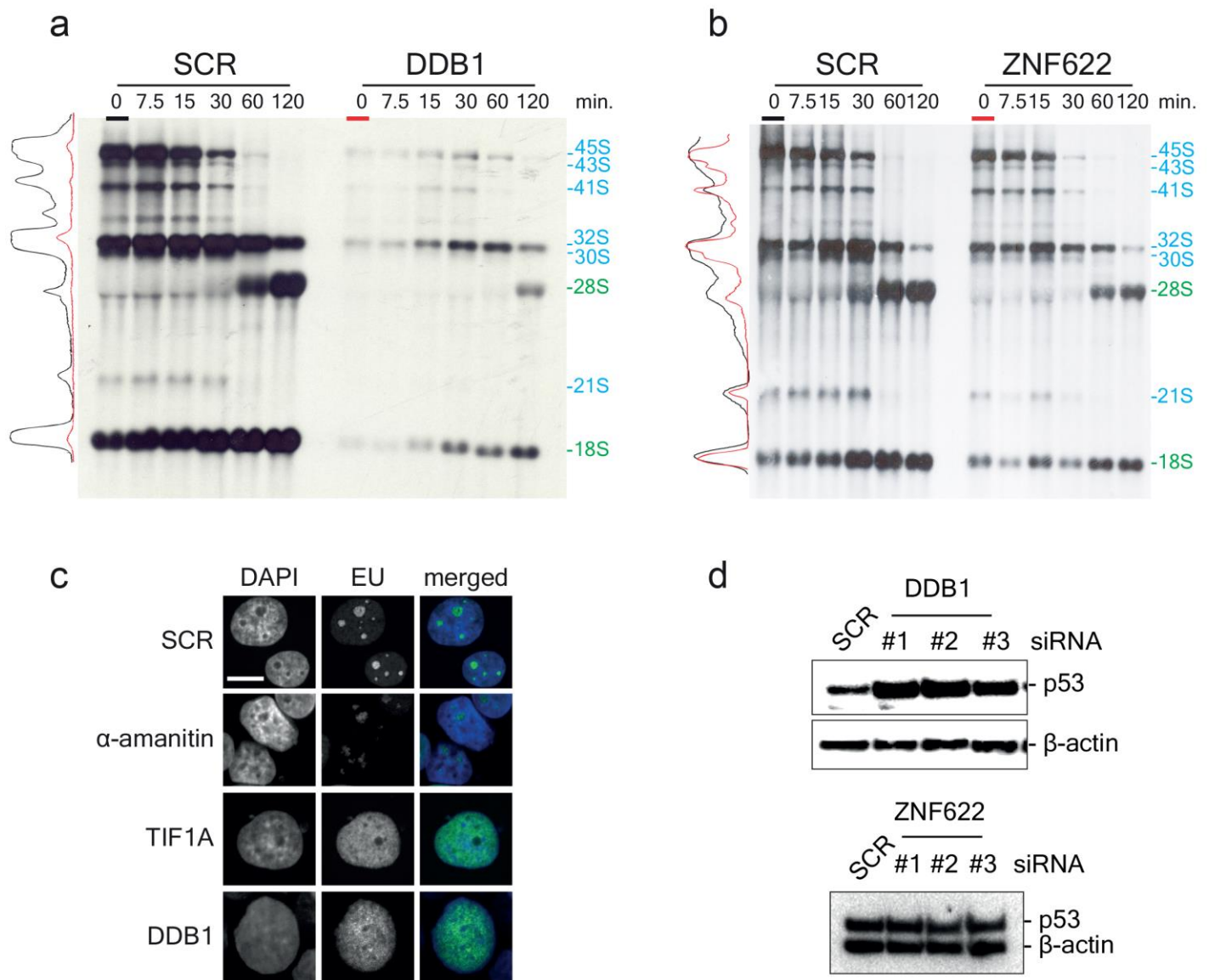
1. Nicolas, E. et al. *Nat. Commun.* **7**, 11390 (2016): <https://www.nature.com/articles/ncomms11390>

In the format provided by the authors and unedited.

Use of the iNo score to discriminate normal from altered nucleolar morphology, with applications in basic cell biology and potential in human disease diagnostics

Vassiliki Stamatopoulou¹, Pascaline Parisot², Christophe De Vleeschouwer² and Denis L. J. Lafontaine ^{3*}

¹Department of Biochemistry, School of Medicine, University of Patras, Patras, Greece. ²ICTEAM-ELEN, Université Catholique de Louvain, Louvain-la-Neuve, Belgium. ³RNA Molecular Biology, F.R.S./FNRS, Université Libre de Bruxelles, Charleroi-Gosselies, Belgium. *e-mail: denis.lafontaine@ulb.ac.be



Supplementary Figure 1

Analysis of the role of DDB1 and ZNF622 in pre-rRNA synthesis, pre-rRNA processing, and nucleolar stress activation

a, b. Dynamic analysis of pre-rRNA synthesis and processing by metabolic pulse-chase labeling. Cells treated for 3 days with an siRNA targeting DDB1 (**a**), or ZNF622 (**b**), or with a non-targeting SCR siRNA control were labeled with tritiated methionine for 30 min and the label was then “chased”, by incubating cells with non-radioactive methionine, for the indicated times. At each time point, total RNA was extracted, resolved by denaturing agarose-gel electrophoresis and analyzed by fluorography. In order to compare RNA synthesis under different conditions, the signal was quantitated with a phosphor imager at the 0-min time point (black profile for cells treated with SCR siRNA, red profiles for DDB1-depleted and ZNF622-depleted cells). Pre-rRNA intermediates (labelled in cyan) and mature rRNAs (the 18S and 28S rRNAs, in green) are indicated. Depletion of DDB1 expression strongly influences the accumulation of the high-molecular-weight RNA species (45S, 43S, 41S). This observation confirms the PCA-based prediction that this protein is required for RNA synthesis (see also flat profile in red). By comparison, ZNF622 expression depletion influences RNA synthesis only marginally. Pre-rRNA processing remains active after

depletion of either proteins (the mature rRNAs 18S and 28S are produced) but it is severely delayed after depletion of DDB1. **c**, *In situ* analysis of RNA synthesis by metabolic labeling. Cells treated for 3 days with an siRNA targeting TIF1A or DDB1 or with a non-targeting SCR siRNA control were incubated for 1 h with 5-ethynyl uridine (EU). EU-labeled RNAs were detected by chemoselective ligation ('click' chemistry). In cells treated with SCR, intense EU signals are detected in the DAPI-counterstained nucleoli (here the signal corresponds to robust RNA Pol I activity) and the DAPI-stained nucleoplasm (where the signal corresponds largely to transcription by RNA Pol II). In cells depleted of TIF1A or DDB1, the nucleolar signal is lost and only the nucleoplasm displays an EU signal. In control cells incubated for 2 h with α -amanitin, which inhibits RNA Pol II, the nucleoplasmic signal is lost while the nucleolar staining remains. DNA was labeled with DAPI. Scale bar: 10 μ m. **d**, nucleolar stress activation assessed by western-blot detection of the p53 steady-state level. Three independent siRNAs (#1, #2, #3) were used to deplete the expression of target proteins DDB1 or ZNF622 for 3 days. DDB1 depletion, which severely inhibits rRNA synthesis (see panels a and c), leads to a marked activation of nucleolar stress (p53 accumulation). By contrast, ZNF622 depletion, which only marginally affects pre-rRNA synthesis and processing (panel b), does not activate nucleolar stress. As loading controls, blots were probed for β -actin.